World Journal of Mechanics, 2012, 2, 42-50
doi:10.4236/wjm.2012.21006 Published Online February 2012 (http://www.SciRP.org/journal/wjm)

Hard-to-Soft Transition in Radial Buckling of Multi-Concentric Nanocylinders

Sung-Jin Park[1], Motohiro Sato[2*], Tetsuro Ikeda[3], Hiroyuki Shima[4,5]
[1]Department of Urban and Environment Engineering, University of Incheon, Incheon, Korea
[2]Division of Engineering and Policy for Sustainable Environment, Faculty of Engineering, Hokkaido University, Sapporo, Japan
[3]Division of Engineering and Policy for Sustainable Environment, Graduate School of Engineering, Hokkaido University, Sapporo, Japan
[4]Division of Applied Physics, Faculty of Engineering, Hokkaido University, Sapporo, Japan
[5]Department of Environmental Sciences, University of Yamanashi, Kofu, Japan
Email: *tayu@eng.hokudai.ac.jp

Received November 29, 2011; revised January 5, 2012; accepted January 15, 2012

ABSTRACT

We investigate the cross-sectional buckling of multi-concentric tubular nanomaterials, which are called multiwalled carbon nanotubes (MWNTs), using an analysis based on thin-shell theory. MWNTs under hydrostatic pressure experience radial buckling. As a result of this, different buckling modes are obtained depending on the inter-tube separation d as well as the number of constituent tubes N and the innermost tube diameter. All of the buckling modes are classified into two deformation phases. In the first phase, which corresponds to an elliptic deformation, the radial stiffness increases rapidly with increasing N. In contrast, the second phase yields wavy, corrugated structures along the circumference for which the radial stiffness declines with increasing N. The hard-to-soft phase transition in radial buckling is a direct consequence of the core-shell structure of MWNTs. Special attention is devoted to how the variation in d affects the critical tube number N_c, which separates the two deformation phases observed in N -walled nanotubes, *i.e.*, the elliptic phase for $N < N_c$ and the corrugated phase for $N > N_c$. We demonstrate that a larger d tends to result in a smaller N_c, which is attributed to the primary role of the interatomic forces between concentric tubes in the hard-to-soft transition during the radial buckling of MWNTs.

Keywords: Carbon Nanotube; Buckling; Radial Corrugation; High Pressure Phenomenon; Van der Waals Coupling; Multiple Core-Shell Structure; Thin Shell Theory

1. Introduction

The term "buckling" refers to a deformation through which a pressurized material undergoes a sudden failure and exhibits a large displacement in a direction transverse to the load [1]. A typical example of buckling occurs when pressing opposite edges of a long, thin elastic beam toward one another. For small loads, the beam is compressed in the axial direction while keeping its linear shape and the strain energy is proportional to the square of the axial displacement. Beyond a certain critical load, however, it suddenly bends into an arc shape and the strain energy and displacements are no longer related by a quadratic expression. Besides axial compression, bending and torsion give rise to buckling of elastic objects, where the buckled patterns depend strongly on the geometric and material parameters.

An interesting class of elastic buckling can be observed in structural pipe-in-pipe cross sections under hydrostatic pressure [2,3]. Pipe-in-pipe (*i.e.*, a pipe inserted inside another pipe) applications are commonly used in offshore oil and gas production systems in civil engineering. In subsea pipelines in deep water, for instance, buckling resistance to huge external hydrostatic pressure is a key structural design requirement. Pipe-in-pipe systems may be an efficient design solution that meets this strict requirement, because their concentric structures enable the cross section to withstand high pressure without collapsing.

The above argument regarding macroscopic objects poses a question as to what buckling behavior may be observed in nanometer-scale (10^{-9} m) counterpart objects. In nanomaterial sciences, the buckling of carbon-based hollow cylinders with nanometric diameters (called carbon nanotubes) has drawn great attention [4]. Extensive studies on carbon nanotube mechanics have been thus far driven by their exceptional resilience against deformation;

*Corresponding author.

that is, the recovery of the original cylindrical shapes of the carbon nanotubes upon unloading, even when subjected to severe loading conditions. In addition to the excellent strain-relaxation reversibility, carbon nanotubes exhibit high fatigue resistance; therefore, they are a promising medium for the storage of mechanical energy with an extremely high energy density [5]. Nevertheless, due to their nanometric scales, the similarities and differences in the buckling patterns compared with those of their macroscopic counterparts are not trivial. This complexity has motivated tremendous efforts toward the analysis of the buckling of carbon nanotubes under diverse loading conditions: axial compression [6-10], radial compression [11-22], bending [23-28], torsion [29-32], and combinations of these [33].

In this article, we focus our attention on the radial buckling of carbon nanotubes observed under hydrostatic pressure on the order of several hundreds of megapascal. Thin-shell-theory based analysis on the cross-sectional deformation of nanotubes leads us to the conclusion that the buckled patterns strongly depend on the inter-tube separation d, the number of constituent tubes N, and the innermost tube diameter D. In particular, the expansion of d from its equilibrium value (0.34 nm) causes a lowering of the critical tube number N_c that characterizes the hard-to-soft transition in the nanotubes' radial buckling. These results shed light on the possible control of the morphology of carbon nanotubes by experimentally tuning d.

2. What Are "Carbon Nanotubes"?

Carbon nanotubes are one of the most promising nanomaterials, and they consist of layers of graphene sheets that are each a single atom thick (two-dimensional hexagonal lattices of carbon atoms) rolled up into concentric cylinders [34]. By convention, they are categorized as single-walled nanotubes (SWNTs) or multi-walled nanotubes (MWNTs): the former is made by wrapping one single layer into one seamless cylinder, while the latter comprise two or more concentric graphitic tubes. The constituent tubes in MWNTs are coupled to one another via the van der Waals (vdW) interaction, wherein the separation between adjacent concentric tubes is approximately 0.34 nm in equilibrium conditions.

The excellent mechanical properties of carbon nanotubes are characterized by the remarkably high Young's modulus, which is on the order of terapascal (*i.e.*, several times stiffer than steel), and the tensile strength, which is as high as tens of gigapascal [33]. These properties are proof that carbon nanotubes are the stiffest and strongest materials on earth. In addition to the marked stiffness, carbon nanotubes exhibit astounding flexibility when subjected to external hydrostatic pressure. The radial deformation both of SWNTs and MWNTs is an important consequence of this flexibility; however, the theoretical understanding of the flexibility of MWNTs is still lacking due to their structural complexity.

Emphasis should be placed on the fact that on application of a mechanical deformation, carbon nanotubes show significant changes in their physical and chemical properties [34,35]. Precise knowledge of their deformation mechanism and available geometry is, therefore, crucial for understanding their structure-property relations and for developing next generation carbon-nanotube-based applications.

3. Formulation

3.1. Continuum Approximation

The aim of this section is to deduce the stable cross-sectional shape of a MWNT under a hydrostatic pressure p. The continuum elastic approximation [36-41] allows the mechanical energy U of a MWNT per axial length to be expressed as follows:

$$U = U\left[p, u_i(p,\theta), v_i(p,\theta)\right] = U_D + U_I + \Omega. \tag{1}$$

Here, U_D is the deformation energy of all concentric tubes, U_I is the interaction energy of all adjacent pairs of tubes, and Ω is the potential energy of the applied pressure. All these three energy terms are functions of p and the deformation amplitudes $u_i(p,\theta)$ and $v_i(p,\theta)$ that describe the radial (r) and circumferential (θ) displacements, respectively, of the i th tube. See Equation (7) below for the precise definitions of u_i and v_i.

The optimal displacements u_i and v_i that minimize U under a given p are obtained via the calculus of variations to U with respect to u_i and v_i. To proceed, we derive the explicit forms of U_D, U_I, and Ω as functions of u_i, v_i, and p in the subsequent section.

3.2. Strain-Displacement Relation

Evaluating the functional form of U_D requires the relation between the displacements, u_i and v_i, and the circumferential strain, $\tilde{\varepsilon}$, of a hollow tube driven by cross-sectional deformation. Suppose there is a circumferential line element of length[1] $d\tilde{\ell}$ lying at an arbitrary point within the cross section of a tube with thickness h. The hydrostatic pressure p upon the tube causes an extensional strain $\tilde{\varepsilon}$ of the line element, which is de-

[1]Throughout this subsection, the tilde $(\tilde{\ })$ attached to variables indicates to take a quantity at arbitrary point within the cross section of the h-thickness tube. On the other hand, variables with no tilde indicates the quantity just on the centroidal arc of the h-thickness tube. See the difference between $\tilde{\varepsilon}$ and ε given in Equation (8) for a clear example.

fined as follows:

$$\tilde{\varepsilon} = \frac{\mathrm{d}\tilde{\ell}^* - \mathrm{d}\tilde{\ell}}{\mathrm{d}\tilde{\ell}}. \quad (2)$$

Here, $\mathrm{d}\tilde{\ell} = \tilde{r}\mathrm{d}\theta$, and $\mathrm{d}\tilde{\ell}^*$ is the length of the line element after deformation (the asterisk symbolizes the quantity after deformation). The coordinates $\tilde{x}^*$, $\tilde{y}^*$ of the element after deformation are given as follows:

$$\tilde{x}^*(\tilde{r},\theta) = \left[\tilde{r} + \tilde{u}(\theta)\right]\cos\theta - \tilde{v}(\theta)\sin\theta, \quad (3)$$

$$\tilde{y}^*(\tilde{r},\theta) = \left[\tilde{r} + \tilde{u}(\theta)\right]\sin\theta + \tilde{v}(\theta)\cos\theta, \quad (4)$$

where $\tilde{u}$ and $\tilde{v}$ are the components of the displacement vector in the radial and circumferential directions, respectively. We can then write the following relationships:

$$\left(d\tilde{\ell}^*\right)^2 = \left(d\tilde{x}^*\right)^2 + \left(d\tilde{y}^*\right)^2, \quad (5)$$

the following relationship can be obtained:

$$\tilde{\varepsilon} = \frac{\tilde{u} + \tilde{v}'}{\tilde{r}} + \frac{1}{2}\left(\frac{\tilde{u} + \tilde{v}'}{\tilde{r}}\right)^2 + \frac{\beta^2}{2}, \quad (6)$$

where $\tilde{u}' \equiv \mathrm{d}\tilde{u}/\mathrm{d}\theta$, *etc*. The term $\beta = (\tilde{v} - \tilde{u}')/\tilde{r}$ in Equation (6) accounts for the rotation of the line element due to the deformation [16]. The formula (6) is valid for an arbitrarily large rotation, β.

Hereafter, we assume that $\tilde{\varepsilon}$ and β are both significantly smaller than unity, because an infinitesimal deflection of the initially circular cross section is assumed to determine the critical buckling pressure. The second term in the right side in Equation (6) can therefore be omitted if the possibility that $|\tilde{u}|$ or $|\tilde{v}'|$ is larger than $\tilde{r}$ is excluded. We further assume that the normals to the undeformed centroidal circle C of the hollow tube's cross section remain straight, normal, and unextended during the deformation [16]. The second assumption means that within each cross section, neither shear deformation nor thickness modulation arises in the circumferential direction; this leads to the following expressions:

$$\tilde{u} = u \text{ and } \tilde{v} = v + z\beta, \quad (7)$$

where u and v denote the displacements of a point that lies on C, and z is a radial coordinate measured from C. By substituting Equation (7) into Equation (6), we can derive the following strain-displacement relationship:

$$\tilde{\varepsilon}(z,\theta) = \varepsilon(\theta) + z\kappa(\theta), \quad (8)$$

where the following definitions hold true:

$$\varepsilon = \frac{u + v'}{r} + \frac{1}{2}\left(\frac{u' - v}{r}\right)^2 \text{ and } \kappa = -\frac{u'' - v'}{r^2}. \quad (9)$$

Here, ε_i and κ_i are the in-plane and bending strains, respectively, of the i th tube; r is the radius of the undeformed circle C. Equations (8) and (9) state that the circumferential strain at an arbitrary point in the cross section is determined by the displacements $u(\theta)$ and $v(\theta)$ of a point that lies on the undeformed centroidal circle C.

3.3. Deformation Energy

We are now ready to derive the explicit form of the deformation energy U_D. Suppose that the i th constituent tube has a thickness h. A surface element of the cross-section of the hollow tube can then be expressed by $r_i \mathrm{d}\theta \mathrm{d}z$. The stiffness k of the surface element for stretching along the circumferential direction is given as follows:

$$k = \frac{E}{1 - \nu^2}, \quad (10)$$

where E and ν are the Young's modulus and Poisson's ratio, respectively, of the tube. Thus, the deformation energy U_D per axial length can be written as follows:

$$U_D = \sum_{i=1}^{N} U_D^{(i)}, \quad (11)$$

in which the component $U_D^{(i)}$ associated with the i th tube is written as follows:

$$U_D^{(i)} = \frac{kr_i}{2}\int_{-h/2}^{h/2}\int_0^{2\pi} \tilde{\varepsilon}_i(z,\theta)^2 \,\mathrm{d}z\mathrm{d}\theta. \quad (12)$$

From Equations (8) and (12) we obtain the following relationship:

$$U_D^{(i)} = \frac{khr_i}{2}\int_0^{2\pi} \varepsilon_i^2 \mathrm{d}\theta + \frac{kh^3 r_i}{24}\int_0^{2\pi} \kappa_i^2 \mathrm{d}\theta, \quad (13)$$

which can also be written as follows:

$$U_D^{(i)} = \frac{r_i}{2}\left(\frac{\Lambda}{1 - \nu^2}\int_0^{2\pi} \varepsilon_i^2 \mathrm{d}\theta + \Phi\int_0^{2\pi} \kappa_i^2 \mathrm{d}\theta\right). \quad (14)$$

The constant Λ denotes the in-plane stiffness, Φ the flexural rigidity, and ν the Poisson ratio of each tube.

For quantitative discussions, the values of Λ and Φ must be carefully determined. In cases of macroscopic objects, they are defined as $\Lambda = Eh$ and $\Phi = Eh^3 / \left[12\left(1 - \nu^2\right)\right]$. However, for carbon nanotubes, the macroscopic relations for Λ and Φ noted above fail because there is no unique way of defining the thickness of the graphene tube [42][2] Thus, the values of Λ and Φ should be evaluated ab-initio from direct measurements or through computations involving the properties of carbon sheets, without reference to the macroscopic relations. In actual calculations, we substi-

[2]The tube is made out of a monoatomic graphitic layer, and consequently, the notion of a tube thickness becomes elusive.

tute $\Lambda = 345$ nN/nm, $\Phi = 0.238$ nN·nm, and $\nu = 0.149$ in a similar fashion as a previous study [43] based on the density functional theory.

3.4. Inter-Tube Coupling Energy

The energy associated with the van der Waals (vdW) interaction between adjacent pairs of tubes, designated by U_I in Equation (1), can be written as a sum of components as follows:

$$U_I = \sum_{i=1}^{N} \sum_{j \neq i} U_I^{(i,j)}, \qquad U_I^{(i,j)} = \frac{c_{i,j}\left(r_i + r_j\right)}{4} \int_0^{2\pi} \left(u_i - u_j\right)^2 \mathrm{d}\theta. \tag{15}$$

We derive the coefficients $c_{i,j}$ in Equation (15) through a first order Taylor approximation of the vdW pressure [39,44] associated with the vdW potential as follows:

$$V(\xi) = 4\varepsilon \left[\left(\frac{\sigma}{\xi} \right)^{12} - \left(\frac{\sigma}{\xi} \right)^{6} \right]. \tag{16}$$

Here, ξ is the distance between a pair of carbon atoms, $2^{1/6}\sigma = 0.383$ nm is the equilibrium distance between two interacting atoms, and $\varepsilon = 0.383 \times 10^{-3}$ nN·nm is the well depth of the potential [45]. The resulting equilibrium spacing between neighboring tubes is 0.3415 nm. The derivative $F = \partial V / \partial \xi$ represents the force between two carbon atoms, and its surface integral provides the inter-wall pressure induced by the vdW coupling.

The vdW pressures on the inner and outer tubes of a concentric two-walled tube with radii r_{inn} and r_{out} are given as follows [44] (with positive signs for compression):

$$p_{\text{inn}} = \alpha \frac{r_{\text{out}}}{r_{\text{inn}}} f_- \quad \text{and} \quad p_{\text{out}} = \alpha \frac{r_{\text{inn}}}{r_{\text{out}}} f_+, \tag{17}$$

where $\alpha = 3\pi\varepsilon\sigma\rho_c^2/32$. The area density of carbon atoms is given by $\rho_c = 38.18$ nm^{-2}.

$$f_\pm = 231\beta^{11}\left(\gamma E_{13} \pm E_{11}\right) - 160\beta^5\left(\gamma E_7 \pm E_5\right). \tag{18}$$

In Equation (18), $\beta = \sigma / \left(r_{\text{out}} + r_{\text{inn}}\right)$, $\gamma = h / \left(r_{\text{out}} + r_{\text{inn}}\right)$, $h = r_{\text{out}} - r_{\text{inn}}$, and $E_m = \int_0^{\pi/2} \left(1 - k^2 \sin^2\theta\right)^{-m/2} \mathrm{d}\theta$, and $k = 4 r_{\text{inn}} r_{\text{out}} / \left(r_{\text{inn}} + r_{\text{out}}\right)^2$.

In the following, we obtain analytical expressions for $c_{i,j}$ by linearizing the Equation (17) for the pressure [22]. Note that $U_I^{(i,j)}$ depends quadratically on the change in spacing between two adjacent tubes. Consider two consecutive tubes with radii r_i and r_{i+1}, where the subscripts i and $i+1$ correspond to inn and out, respectively. The vdW energy stored due to a perturbation $\Delta\mathrm{d}$ along the positive direction of pressure is given as follows:

$$U_I^{(i,i+1)} \approx \frac{r_{\text{m}}}{2} \int_0^{2\pi} \left(-p_{i,i+1} \frac{\Delta\mathrm{d}}{2} - p_{i+1,i} \frac{\Delta\mathrm{d}}{2} \right) \mathrm{d}\theta, \tag{19}$$

where $r_{\text{m}} = \left(r_i + r_{i+1}\right)/2$ is the mean radius and $p_{i,i+1}$ is the vdW pressure on the i th tube. The corresponding linearized pressure is given by $\partial p_{i,i+1} / \partial d \big|_{r_{\text{m}}}$. In Equation (19), $r_{\text{m}}\mathrm{d}\theta$ describes the length of the infinitesimal element on which the pressure is acting. Using the linearized pressure and comparing with Equation (15), the following expressions for the vdW coefficients can be found:

$$c_{i,i+1} = -\frac{1}{4} \left(\frac{\partial p_{i,i+1}}{\partial d} + \frac{\partial p_{i+1,i}}{\partial d} \right), \tag{20}$$

where the derivatives in Equation (20) are defined as follows:

$$\begin{aligned} \partial p_{\text{i,i+1}} \partial d \big|_{r_{\text{m}}} &= 2\alpha\, r_{\text{m}} \left(r_{\text{m}} - d/2\right)^2 f_- \\ &\quad + \alpha \left(\frac{r_{\text{m}} + d/2}{r_{\text{m}} - d/2} \right) \partial f_- \partial d, \\ \partial p_{\text{i+1,i}} \partial d \big|_{r_{\text{m}}} &= -2\alpha\, r_{\text{m}} \left(r_{\text{m}} + d/2\right)^2 f_+ \\ &\quad + \alpha \left(\frac{r_{\text{m}} - d/2}{r_{\text{m}} + d/2} \right) \partial f_+ \partial d. \end{aligned} \tag{21}$$

Note that $c_{i,j}$ is symmetric. The set of Equations (15), (20), and (21) allows for the evaluation of U_I.

3.5. Pressure-Induced Energy

We finally derive an explicit form of Ω, which is the negative of the work done by the external pressure p during cross-sectional deformation. Using this definition we can write the following expression:

$$\Omega = -p\left(\pi r_N^2 - S^*\right), \tag{22}$$

where S^* is the area surrounded by the N th tube after deformation (the sign of p is assumed to be positive inward). S^* can then be obtained by evaluating the following expression:

$$S^* = \frac{1}{2} \int_0^{2\pi} \left(x_N^* y_N^{*\prime} - y_N^* x_N^{*\prime} \right) \mathrm{d}\theta. \tag{23}$$

By substituting Equations (3) and (4) into Equation (23), and by using the periodicity relation $\int_0^{2\pi} v_N' \mathrm{d}\theta = 0$, the following expression can be obtained:

$$\Omega = p \int_0^{2\pi} \left(r_N u_N + \frac{u_N^2 + v_N^2 - u_N' v_N + u_N v_N'}{2} \right) \mathrm{d}\theta. \tag{24}$$

3.6. Critical Pressure Evaluation

This section presents our method for determining the critical pressure p_c above which the circular cross section of MWNTs is elastically deformed into a non-circular one. To carry out this analysis, we decompose the radial displacement terms according to $u_i(p,\theta) = u_i^{(0)}(p) + \delta u_i(\theta)$. Here, $u_i^{(0)}(p)$ indicates a uniform radial contraction of the ith tube at $p < p_c$, whose magnitude is proportional to p. $\delta u_i(\theta)$ describes a deformed, non-circular cross section observed just above p_c. Similarly, we can write $v_i(p,\theta) = \delta v_i(\theta)$, because $v_i^{(0)}(p) \equiv 0$ at $p < p_c$.

By applying the variational method to U with respect to u_i and v_i, we obtain the following system of $2N$ linear differential equations:

$$\begin{aligned}
&\alpha_i\left(\delta u_i + \delta v_i - \gamma_i \eta_i\right) + \beta_i \eta_i + p\delta_{i,N}\left(\delta u_i + \delta v_i\right) \\
&+\left(1-\delta_{i,N}\right) c_{i,i+1} r_i \left(\delta u_i - \delta u_{i+1}\right) \\
&+\left(1-\delta_{i,1}\right) c_{i,i-1} r_i \left(\delta u_i - \delta u_{i-1}\right) = 0,
\end{aligned} \tag{25}$$

$$\begin{aligned}
&\alpha_i\left(\delta u_i + \delta v_i + \gamma_i \eta_i\right) - \beta_i \eta_i \\
&+ p\delta_{i,N}\left(\delta u_i - \delta v_i\right) = 0,
\end{aligned} \tag{26}$$

where $\gamma_i = u_i^{(0)}(p)/r_i$ and $\eta_i = u_i - v_i$. In deriving Equations (25) and (26), the quadratic and cubic terms in δu_i and δv_i are omitted because we only consider elastic deformation with sufficiently small displacements. In addition, the terms consisting only of $u_i^{(0)}$ and p are also omitted; the sum of such terms should be equal to zero[3] because $u_i^{(0)}$ represents an equilibrium circular cross-section under p.

Because δu_i and δv_i are periodic in θ, the general solutions of Equations (25) and (26) are given by the Fourier series expansions as follows:

$$\delta u_i(\theta) = \sum_{n=1}^{\infty} \delta \bar{\mu}_i(n) \cos n\theta$$

$$\text{and } \delta v_i(\theta) = \sum_{n=1}^{\infty} \delta \bar{\nu}_i(n) \sin n\theta.$$

Substituting these into Equations (25) and (26) leads to the matrix equation $\mathbf{Mu} = \mathbf{0}$, in which the vector $\mathbf{u}$ consists of $\delta\bar{\mu}_i(n)$ and $\delta\bar{\nu}_i(n)$ with all possible i and n, and the matrix $\mathbf{M}$ involves one variable p as well as parameters such as α_i and β_i. The matrix $\mathbf{M}$ can be expressed as a block diagonal matrix of the form $\mathbf{M} = \mathbf{M}_{n=1} \oplus \mathbf{M}_{n=2} \oplus \cdots$ due to the orthogonality of $\cos n\theta$ and $\sin n\theta$. Here, $\mathbf{M}_{n=m}$ is a $2N \times 2N$ submatrix that satisfies $\mathbf{M}_{n=m}\mathbf{u}_{n=m} = 0$, where $\mathbf{u}_{n=m}$ is a $2N$-column vector composed of $\delta\bar{\mu}_i(n=m)$ and $\delta\bar{\nu}_i(n=m)$. As a result, the secular equation $\det(\mathbf{M}) = 0$ that provides nontrivial solutions of Equations (25) and (26) can be rewritten as follows:

$$\det\left(\mathbf{M}_{n=1}\right)\det\left(\mathbf{M}_{n=2}\right)\cdots = 0. \tag{27}$$

By solving Equation (27) with respect to p, we obtain a sequence of discrete values of p. Each of these values is the smallest solution of $\det(\mathbf{M}_{n=m})\cdots = 0$ $(m = 1, 2, \cdots)$. The minimum of these values serves as the critical pressure p_c that is associated with a specific integer $n = m$. From the definition, the p_c associated with a specific m allows only $\delta\bar{\mu}_i(n=m)$ and $\delta\bar{\nu}_i(n=m)$ to be finite, however, it also requires $\delta\bar{\mu}_i(n \ne m) \equiv 0$ and $\delta\bar{\nu}_i(n \ne m) \equiv 0$. Immediately above p_c, therefore, the circular cross section of MWNTs becomes radially deformed as follows:

$$\begin{aligned}
&u_i(\theta) = u_i^{(0)}(p_c) + \delta\bar{\mu}_i(n)\cos n\theta \\
&\text{and} \\
&v_i(\theta) = \delta\bar{\nu}_i(n)\sin n\theta,
\end{aligned} \tag{28}$$

where the value of n is uniquely determined by the one-to-one relation between n and p_c.

4. Result and Discussion

4.1. Critical Pressure Curve

Figures 1(a) and **(b)** show p_c as a function of N for various values of the initial tube-tube separation d prior to the application of pressure. For all d, we observe a rapid increase in p_c with N, which is followed by a slow decay when $D = 3.0$ nm (and also for smaller D).[4] The increase in p_c for small N is interpreted as the "hardening" of the MWNTs, *i.e.*, an enhancement of the radial stiffness of the entire MWNT by encapsulation. This hardening effect disappears with a further increase in N, which results in the decay of $p_c(N)$. A decay in p_c implies that a relatively low pressure suffices to produce a radial deformation, which indicates an effective "softening" of the MWNT. These two contrasting effects, *i.e.*, hardening and softening, are both due to the encapsulation of MWNTs.

We emphasize that in **Figure 1(a)**, the softening region (*i.e.*, p_c-decay region) is enlarged by expanding the inter-tube distance d prior to deformation. As will be confirmed later, this tendency agrees with the existing numerical simulations that were based on a coarse-grained model of MWNTs [21]. The variation of d is thought to be feasible in MWNT synthesis. During synthesis, the interlayer thermal contraction upon cooling and/or the intertube adhesion energy owing to the increased intertube commensuration may result in a deviation in d from the equilibrium value [46,47].

4.2. Sequential Change in Buckling Modes

Figure 2 provides **(a)** the index n of deformation modes and **(b)-(g)** the cross-sectional views observed just

[3]The fact that the sum equals zero determines the functional form of $u_i^{(0)}(p)$.

[4]Such a decay is also observed for D = 5.0 nm and larger D, in principle if a sufficiently large N is considered [but omitted in **Figure 1(b)**].

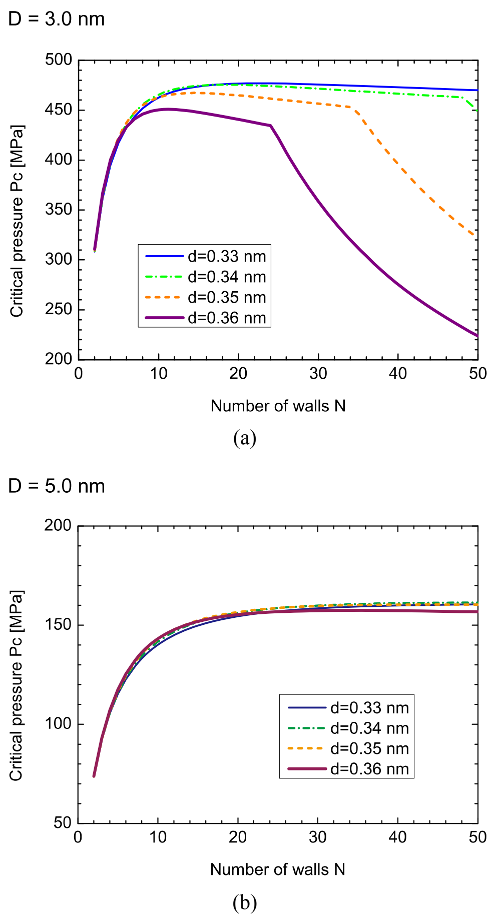

Figure 1. (Color online) Critical pressure curves showing P_c required to produce radial deformation of *N*-walled nanotubes with fixed *D*: (a) *D* = 3.0 nm, and (b) *D* = 5.0 nm.

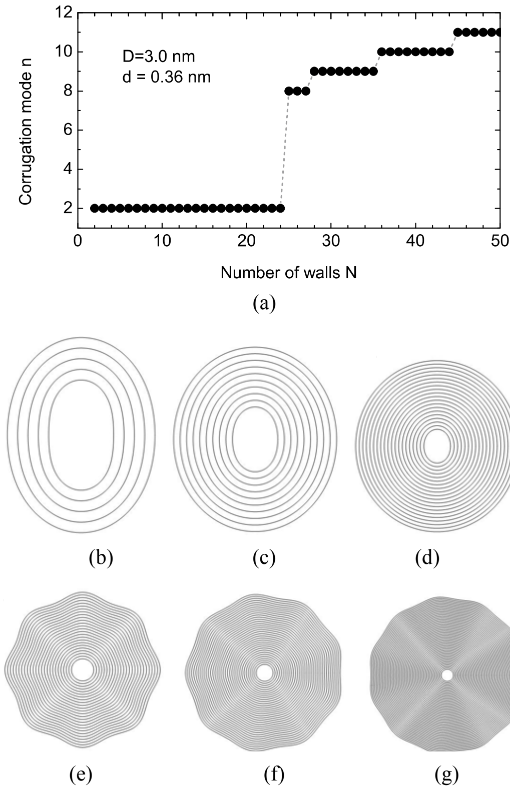

Figure 2. [Upper panel] (a) Stepwise increase in the index *n* of radial buckling modes. The index *n* indicates the circumferential wave number of the deformed cross-section. [Bottom panel] Cross-sectional views of buckled MWNTs under high hydrostatic pressure: (b)-(d) Elliptic deformation mode (*n* = 2) for *N* = 5, 10, 20; (e) Radial corrugation mode with *n* = 8 for *N* = 25; (f) *n* = 9 for *N* = 35; (g) *n* = 11 for *N* = 50.

above p_c for fixed $D \equiv 3.0$ nm and $d \equiv 0.36$ nm. The most striking observation is the successive transformation of the cross section with an increase in N. We see from **Figure 2(a)** that the deformation mode observed just above p_c jumps abruptly from $n = 2$ to n = 8 at $N = 25$, which is followed by successive emergences of higher corrugation modes with larger n. These transitions in n originate from the two competing effects inherent in MWNTs with $N = 1$, that is, the relative rigidity of the inner tubes and the mechanical instability of the outer tubes. A large discrepancy in the radial stiffness of the inner and outer tubes gives rise to an uneven distribution of the deformation amplitudes of concentric tubes that interact through the vdW forces, which consequently produces an abrupt change in the observed deformation mode at some N.

4.3. Hard-to-Soft Transition

Of further interest is that the critical number of tubes $N = N_c$ separating the elliptic phase ($n = 2$) from the corrugation phase ($n \geq 3$) is identified as the N that yields a cusp in the curve of $p_c(N)$ [see **Figure 1(a)**]. In contrast, no singularity is observed in the curve of $p_c(N)$ at any value of N, which separates two neighboring corrugation phases. We emphasize that at these phase boundaries, one additional tube induces a drastic change in the cross-sectional shape of the MWNT under hydrostatic pressure.

Figure 3 explains why the singular cusp in the $p_c(N)$ curve corresponds to the hard-to-soft transition point of $N = N_c$. This figure shows the *N*-dependence of the solutions $p(N)$ for the secular equation $\det(\mathbf{M}) = 0$. As mentioned earlier, the secular equation provides various values of p. Each of these values is associated with a specific mode index n. The minimum value of p gives the critical pressure p_c just above which cross-sectional deformation takes place. **Figure 3** depicts the *N*-dependence of $p(N)$ for several n values, where the innermost tube radius is fixed to be $D = 3.0$ nm. For $N \leq 24$, the values of p for $n = 2$ are less than those for $n \geq 3$, which implies that the elliptic mode occurs for MWNTs with $N \leq 24$. However, at $N = 25$ (and $N = 26, 27$), the minimum p corre-

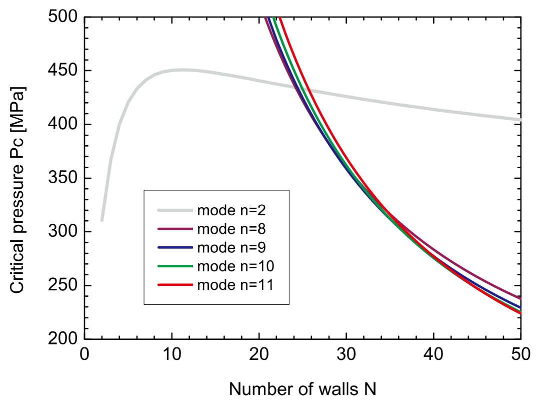

Figure 3. Branches of solutions *p*(*N*) for the secular equation det(M) = 0 (refer text). The innermost tube diameter is set to be *D* = 3.0 nm for all curves. For a fixed *N*, the minimum value of *p* among the branches takes a role of the critical pressure p_c at that *N*.

sponds to $n=8$, which implies the occurrence of the corrugation mode of $n=8$. It should be noted that p for $3 \le n \le 7$ can never attain the minimum value at any N. This is why the corrugation mode of n with $3 \le n \le 7$ cannot be observed for MWNTs with $D=3.0$ nm. It also follows from **Figure 3** that the cusps in the curves $p_c(N)$ occur only at the phase boundary N_c separating the elliptic phase $(n=2)$ from a corrugation phase $(n \ge 8)$, while no singularity appears at the boundaries of N between neighboring corrugation phases.

5. Summary

A thin-shell-theory based analysis has been employed to detect the mechanical hard-to-soft transition relevant to the radial buckling of MWNTs subject to hydrostatic pressure. Various buckled patterns are found to be available, and the parameters d, N, and D strongly influence which pattern is energetically favored. We have evaluated the phase boundary N_c and the critical pressure p_c for several pairs of d and D, revealing that the artificial expansion of d results in a decrease in N_c. Further studies will shed light on other mechanical properties of MWNTs and suggest applications based on their unique cross-sectional deformations.

6. Acknowledgements

The fruitful discussion with S. Ghosh and M. Arroyo on the vdW-interaction formulas is greatly acknowledged. This work was supported by KAKENHI from MEXT, Japan. HS cordially thanks the Inamori Foundation and the Suhara Memorial Foundation for financial support.

REFERENCES

[1] D. O. Brush and B. O. Almroth, "Buckling of Bars, Plates, and Shells," McGraw-Hill, New York, 1975.

[2] M. Sato and M. H. Patel, "Exact and Simplified Estimations for Elastic Buckling Pressures of Structural Pipe-in-Pipe Cross Sections under External Hydrostatic Pressure," *Journal of Marine Science and Technology*, Vol. 12, No. 4, 2007, pp. 251-262. doi:10.1007/s00773-007-0244-y

[3] M. Sato, M. H. Patel and F. Trarieux, "Static Displacement and Elastic Buckling Characteristics of Structural Pipe-in-Pipe Cross-Sections," *Structural Engineering and Mechanics*, Vol. 30, 2008, pp. 263-278.

[4] H. Shima, "Buckling of Carbon Nanotubes: A State of the Art Review," *Materials*, Vol. 5, No. 1, 2012, pp. 47-84. doi:10.3390/ma5010047

[5] R. Zhang, Q. Wen, W. Qian, D. Sheng, Q. Zhang and F. Wei, "Superstrong Ultralong Carbon Nanotubes for Mechanical Energy Storage," *Advanced Materials*, Vol. 23, No. 30, 2011, pp. 3387-3391. doi:10.1002/adma.201100344

[6] B. I. Yakobson, C. J. Brabec and J. Bernholc, "Nanomechanics of Carbon Tubes: Instabilities beyond Linear Response," *Physical Review Letters*, Vol. 76, No. 14, 1996, pp. 2511-2514. doi:10.1103/PhysRevLett.76.2511

[7] C. Q. Ru, "Axially Compressed Buckling of a Double-walled Carbon Nanotube Embedded in an Elastic Medium," *Journal of the Mechanics and Physics of Solids*, Vol. 49, No. 6, 2001, pp. 1265-1279. doi:10.1016/S0022-5096(00)00079-X

[8] B. Ni, S. B. Sinnott, P. T. Mikulski and J. A. Harrison, "Compression of Carbon Nanotubes Filled with C_{60}, CH_4, or Ne: Predictions from Molecular Dynamics Simulations," *Physical Review Letters*, Vol. 88, 2002, pp. 205505: 1-205505:4. doi:10.1103/PhysRevLett.88.205505

[9] M. J. Buehler, J. Kong and H. J. Gao, "Deformation Mechanism of Very Long Single-Wall Carbon Nanotubes Subject to Compressive Loading," *Journal of Engineering Materials and Technology*, Vol. 126, No. 3, 2004, pp. 245-249. doi:10.1115/1.1751181

[10] A. Pantano, M. C. Boyce and D. M. Parks, "Mechanics of Axial Compression of Single- and Multi-Wall Carbon Nanotubes," *Journal of Engineering Materials and Technology*, Vol. 126, No. 3, 2004, pp. 279-284. doi:10.1115/1.1752926

[11] J. Tang, J. C. Qin, T. Sasaki, M. Yudasaka, A. Matsushita and S. Iijima, "Compressibility and Polygonization of Single-Walled Carbon Nanotubes under Hydrostatic Pressure," *Physical Review Letters*, Vol. 85, No. 9, 2000, pp. 1887-1889. doi:10.1103/PhysRevLett.85.1887

[12] A. Pantano, D. M. Parks and M. C. Boyce, "Mechanics of Deformation of Single- and Multi-Wall Carbon Nanotubes," *Journal of the Mechanics and Physics of Solids*, Vol. 52, No. 4, 2004, pp. 789-821. doi:10.1016/j.jmps.2003.08.004

[13] J. A. Elliott, L. K. W. Sandler, A. H. Windle, R. J. Young and M. S. P. Shaffer, "Collapse of Single-Wall Carbon Nanotubes Is Diameter Dependent," *Physical Review Letters*, Vol. 92, 2004, pp. 095501:1-095501:4. doi:10.1103/PhysRevLett.92.095501

[14] H. Shima and M. Sato, "Multiple Radial Corrugations in Multiwall Carbon Nanotubes under Pressure," *Nanotechnology*, Vol. 19, 2008, pp. 495705:1-495705:8. doi:10.1088/0957-4484/19/49/495705

[15] J. Peng, J. Wu, K. C. Hwang, J. Song and Y. Huang, "Can a Single-Wall Carbon Nanotube Be Modeled as a Thin Shell?" *Journal of the Mechanics and Physics of Solids*, Vol. 56, No. 6, 2008, pp. 2213-2224. doi:10.1016/j.jmps.2008.01.004

[16] H. Shima and M. Sato, "Pressure-Induced Structural Transitions in Multi-Walled Carbon Nanotubes," *Physica Status Solidi* (*a*), Vol. 206, 2009, pp. 2228-2233. doi:10.1002/pssa.200881706

[17] M. Sato and H. Shima, "Buckling Characteristics of Multiwalled Carbon Nanotubes under External Pressure," *Interaction and Multiscale Mechanics*: *An International Journal*, Vol. 2, 2009, pp. 209-222.

[18] A. P. M. Barboza, H. Chacham and B. R. A. Neves, "Universal Response of Single-Wall Carbon Nanotubes to Radial Compression," *Physical Review Letters*, Vol. 102, 2009, pp. 025501:1-025501:4. doi:10.1103/PhysRevLett.102.025501

[19] H. Shima, M. Sato, K. Iiboshi, S. Ghosh and M. Arroyo, "Diverse Corrugation Pattern in Radially Shrinking Carbon Nanotubes," *Physical Review B*, Vol. 82, 2010, pp. 085401:1-085401:7. doi:10.1103/PhysRevB.82.085401

[20] M. Sato, H. Shima and K. Iiboshi, "Core-Tube Morphology of Multiwall Carbon Nanotubes," *International Journal of Modern Physics B*, Vol. 24, No. 1-2, 2010, pp. 288-294. doi:10.1142/S0217979210064228

[21] X. Huang, W. Liang and S. Zhang, "Radial Corrugations of Multi-Walled Carbon Nanotubes Driven by Inter-Wall Nonbonding Interactions," *Nanoscale Research Letters*, Vol. 6, 2011, pp. 53-58. doi:10.1007/s11671-010-9801-0

[22] H. Shima, S. Ghosh, M. Arroyo, K. Iiboshi and M. Sato, "Thin-Shell Theory Based Analysis of Radially Pressurized Multiwall Carbon Nanotubes," *Computational Materials Science*, Vol. 52, No. 1, 2012, pp. 90-94. doi:10.1016/j.commatsci.2011.04.005

[23] S. Iijima, C. Brabec, A. Maiti and J. Bernholc, "Structural Flexibility of Carbon Nanotubes," *Journal of Chemical Physics*, Vol. 104, No. 5, 1996, pp. 2089-2092. doi:10.1063/1.470966

[24] M. R. Falvo, G. J. Clary, R. M. Taylor II, V. Chi, F. P. Brooks Jr., S. Washburn and R. Superfine, "Bending and Buckling of Carbon Nanotubes under Large Strain," *Nature*, Vol. 389, 1997, pp. 582-584. doi:10.1038/39282

[25] P. Poncharal, Z. L. Wang, D. Ugarte and W. A. de Heer, "Electrostatic Deflections and Electromechanical Resonances of Carbon Nanotubes," *Science*, Vol. 283, No. 5407, 1999, pp. 1513-1516. doi:10.1126/science.283.5407.1513

[26] Y. Shibutani and S. Ogata, "Mechanical Integrity of Carbon Nanotubes for Bending and Torsion," *Modelling and Simulation in Materials Science and Engineering*, Vol. 12, No. 4, 2004, pp. 599-610. doi:10.1088/0965-0393/12/4/003

[27] A. Kutana and K. P. Giapis, "Transient Deformation Regime in Bending of Single-Walled Carbon Nanotubes," *Physical Review Letters*, Vol. 97, 2006, pp. pp.245501: 1-245501:4. doi:10.1103/PhysRevLett.97.245501

[28] H. K. Yang and X. Wang, "Bending Stability of Multi-Wall Carbon Nanotubes Embedded in an Elastic Medium," *Modelling and Simulation in Materials Science and Engineering*, Vol. 14, No. 1, 2006, pp. 99-116. doi:10.1088/0965-0393/14/1/008

[29] I. Arias and M. Arroyo, "Size-Dependent Nonlinear Elastic Scaling of Multiwalled Carbon Nanotubes," *Physical Review Letters*, Vol. 100, 2008, pp. 085503:1-085503:4. doi:10.1103/PhysRevLett.100.085503

[30] Q. Wang, "Torsional Buckling of Double-Walled Carbon Nanotubes," *Carbon*, Vol. 46, No. 8, 2008, pp. 1172-1174. doi:10.1016/j.carbon.2008.03.025

[31] M. Arroyo and I. Arias, "Rippling and a Phase-Transforming Mesoscopic Model for Multiwalled Carbon Nanotubes," *Journal of the Mechanics and Physics of Solids*, Vol. 56, No. 4, 2008, pp. 1224-1244. doi:10.1016/j.jmps.2007.10.001

[32] B. W. Jeong and S. B. Sinnott, "Unique Buckling Responses of Multi-Walled Carbon Nanotubes Incorporated as Torsion Springs," *Carbon*, Vol. 48, No. 6, 2010, pp. 1697-1701. doi:10.1016/j.carbon.2009.12.048

[33] H. Shima and M. Sato, "Elastic and Plastic Deformation of Carbon Nanotoubes," Pan Stanford Publishing, Singapore, 2012.

[34] R. Saito, M. S. Dresselhaus and G. Dresselhaus, "Physical Properties of Carbon Nanotubes," World Scientific Publishing Company, 1998.

[35] A. Loiseau, P. Launois. P. Petit, S. Roche and J. -P. Salvetat, "Understanding Carbon Nanotubes: From Basics to Application," Springer-Verlag, Berlin, 2006.

[36] C. Q. Ru, "Column Buckling of Multiwalled Carbon Nanotubes with Interlayer Radial Displacements," *Physical Review B*, Vol. 62, 2000, pp. 16962-16967. doi:10.1103/PhysRevB.62.16962

[37] C. Y. Wang, C. Q. Ru and A. Mioduchowski, "Axially Compressed Buckling of Pressured Multiwall Carbon Nanotubes," *International Journal of Solids and Structures*, Vol. 40, No. 15, 2003, pp. 3893-3911. doi:10.1016/S0020-7683(03)00213-0

[38] H. S. Shen, "Postbuckling Prediction of Double-Walled Carbon Nanotubes under Hydrostatic Pressure," *International Journal of Solids and Structures*, Vol. 41, No. 9-10, 2004, pp. 2643-2657. doi:10.1016/j.ijsolstr.2003.11.028

[39] X. Q. He, S. Kitipornchai and K. M. Liew, "Buckling Analysis of Multi-Walled Carbon Nanotubes: A Continuum Model Accounting for van der Waals Interaction," *Journal of the Mechanics and Physics of Solids*, Vol. 53, No. 2, 2005, pp. 303-326. doi:10.1016/j.jmps.2004.08.003

[40] N. Silvestre, "Length Dependence of Critical Measures in Single-Walled Carbon Nanotubes," *International Journal of Solids and Structures*, Vol. 45, No. 18-19, 2008, pp. 4902-4920. doi:10.1016/j.ijsolstr.2008.04.029

[41] N. Silvestre, C. M. Wang, Y. Y. Zhang and Y. Xiang, "Sanders Shell Model for Buckling of Single-Walled Car-

bon Nanotubes with Small Aspect Ratio," *Composite Structures*, Vol. 93, No. 7, 2011, pp. 1683-1691. doi:10.1016/j.compstruct.2011.01.004

[42] S. S. Gupta, F. G. Bosco and R. C. Batra, "Wall Thickness and Elastic Moduli of Single-Walled Carbon Nanotubes from Frequencies of Axial, Torsional and Inextensional Modes of Vibration," *Computational Materials Science*, Vol. 47, 2010, pp. 1049-1059. doi:10.1016/j.commatsci.2009.12.007

[43] K. N. Kudin, G. E. Scuseria and B. I. Yakobson, "C_2F, BN, and C Nanoshell Elasticity from *ab initio* Computations," *Physical Review B*, Vol. 64, 2001, pp. 235406: 1-235406:10. doi:10.1103/PhysRevB.64.235406

[44] W. B. Lu, B. Liu, J. Wu, J. Xiao, K. C. Hwang, S. Y. Fu and Y. Huang, "Continuum Modeling of van der Waals Interactions between Carbon Nanotube Walls," *Applied Physics Letters*, Vol. 94, 2009, pp. 101917:1-101917:3. doi:10.1063/1.3099023

[45] L. A. Girifalco, M. Hodak and R. S. Lee, "Carbon Nanotubes, Buckyballs, Ropes, and a Universal Graphitic Potential," *Physical Review B*, Vol. 62, No. 19, 2000, pp. 13104-13110. doi:10.1103/PhysRevB.62.13104

[46] K. Koziol, M. Shaffer and A. Windle, "Three-Dimensional Internal Order in Multiwalled Carbon Nanotubes Grown by Chemical Vapor Deposition," *Advanced Materials*, Vol. 17, 2005, pp. 760-763. doi:10.1002/adma.200401791

[47] C. Ducati, K. Koziol, S. Friedrichs, T. J. V. Yates, M. S. Shaffer, P. A. Midgley and A. H. Windle, "Crystallographic Order in Multi-Walled Carbon Nanotubes Synthesized in the Presence of Nitrogen," *Small*, Vol. 2, No. 6, 2006, pp. 774-784. doi:10.1002/smll.200500513

